Cardiac pulsation evokes long-range quantum coherence in the conscious brain

Christian Kerskens
Institute of Neuroscience, Trinity College, Dublin, Republic of Ireland

David López Pérez
Institute of Neuroscience, Trinity College, Dublin, Ireland,
Neurocognitive Development Lab and Developmental Psychology Unit,
Faculty of Psychology, University of Warsaw, Warsaw

Abstract

We report long-range zero quantum coherence (ZQC) in 40 volunteers, which were repeatedly evoked by the incoming blood pulse. They were observable for periods of 150-400ms if and only if the volunteer was awake. This direct link to blood pulse and wakefulness suggests that the underlying mechanism of the ZQC is a necessity for consciousness. We show that the ZQC generation by the cardiac pulse is inconsistent with Landau's concept of symmetry-breaking matter. However, the ZQC is compatible with the assumption that its underlying mechanism is a non-local topological entanglement arising from a topological ordered phase transition. Then, topological defects, which exist in biology in numerous ways, can be linked to computing and with that to consciousness.

INTRODUCTION

For many years, numerous researchers have speculated that consciousness and cognition could be based on quantum computing (for an overview see [1]). The main objection towards those ideas is the fact that quantum coherence may not survive in the "hot and wet" brain environment for long enough to be used for computing. For that reason, Penrose and Hameroff [2] have come up with the idea that coherence must be protected suggesting that microtubules may provide such a mechanism.
In 2003, Freedman et al. [3] proved that quantum computing in general could also be based on topological computing which in itself is protected against decoherence. In topological protected quantum computing, topological defects may be dragged around in a topologically ordered medium to manipulate information encoded in non-local entanglement, the main feature of topological order. Topological order is a phase of matter which is inconsistent with the Landau picture of symmetry breaking and which again may be not expected intuitively in a "hot and wet" environment. However, despite its unlikeliness, a medium of topologically ordered states could link topological defects which have been identified in a wide range of biological systems from subcellular actomyosin mixtures [4] to tissue [5–7], not only to processes like apoptotic cell extrusion [7] but rather to consciousness and cognition.
Topological entanglement as found in topological order may be associated with unitary operators that are capable of creating quantum entanglement [8]. Fortunately, quantum coherence, which may be equivalent to quantum entanglement for all practical purposes [9], can be detected in the conscious brain using MRI.

In MRI, quantum coherence of nuclear spins can be observed in two ways; directly using multiple spin echoes (MSEs) [10–12] for long-range multiple quantum coherence (MQC) [13] and indirectly in single-quantum coherence (SQC) signals for short-range quantum coherence via T_1 and T_2 relaxation. A basic MSE sequence consists of asymmetric magnetic field gradients, in contrast to single spin echo (SSE) where symmetry is essential, combined with at least two radio-frequency (RF) pulses [10–12]. For any "classical fluid" , signal-to-noise ratio in MSE, which depends on the probability of long-range multiple quantum coherence, is much lower than in SSE. For example in an optimized zero spin echo (ZSE) sequence, the ratio of ZQC to SQC signals only reaches up to 0.02 at 4 T, experimentally [14, 15]. A SSE sequence could also contain MSEs if repeated fast. So-called crusher gradients (to dephase any SQC signal that remains from the previous excitation) which are added between two image acquisitions (see Figure 1), produce an asymmetry in the subsequent image [16]. In our consecutive EPI time series, only the second readout after an onset could contain an MSEs. The asymmetric gradient

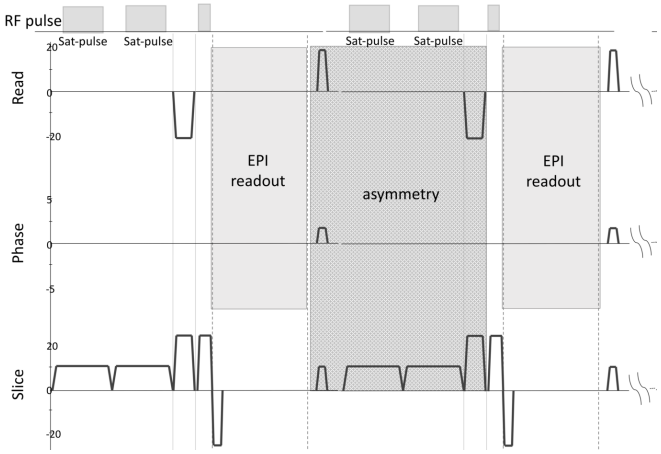

Figure 1. Gradient scheme of two consecutive EPI acquisition. The "asymmetry" field includes all asymmetric gradients of the ZQC.

field as shown in Figure 1) can generate zero quantum orders [14] and higher negative orders [17]. Of course, fast imaging sequences have a high noise level (around 0.02) which means that ZQC signals are negligible in fast imaging series for any classical liquids which is also the intention of the sequence design. Therefore, any MQC signals generated by a conventionally fast imaging sequence may derive from exotic matter, especially, if T_1 and T_2 remain constant excluding short-range effects.

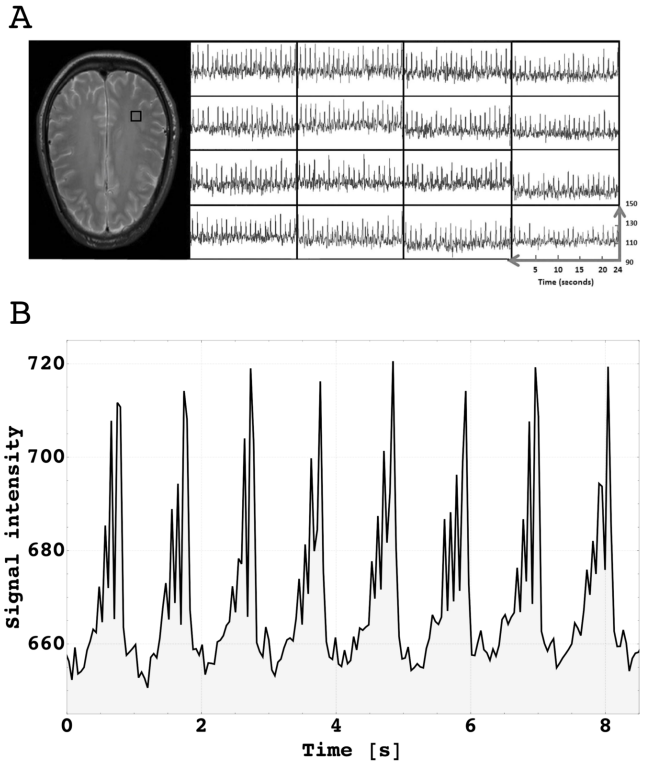

Figure 2. **A**: One 4x4 voxel matrix randomly picked. On the left, the black square shows location in the brain slice. On the right, 16 corresponding signal time courses of 24 s displaying the local tissue responses. **B**: Whole-slice averaged signal time course (selected by a mask) during 8 heart cycles. Subject had extra head fixation and was instructed to breath-hold during the period. In contrast to signals in the veins (not shown here), zigzag signal showed no response to CO2 activity other than an immediate lengthening of the zigzag.

RESULTS

We studied 40 subjects [18] (between 18 and 46 years old) using a 3.0 T Philips whole-body MRI scanner (Philips, The Netherlands) which was operated with a 32-channel array receiver coil. Initial experiments were carried out to establish a protocol that could deliver stable cardiac related signals over a range of subjects. With the finalized gradient-echo echo planar imaging (GE-EPI) sequence [19] we found predominant alternations with the cardiac frequency in brain tissue (Figure 2). In each cardiac cycle, we observed a period, which varied in length between 150 and up to 420 ms under special circumstances Figure 2B, showing an alternating signal of up to 15 % to which we will refer to in the following as zigzags. Under normal condition, the zigzags usually contain two or three peaks as shown in Figure 5B (during the first 10 s from 50 s to 60 s). During our initial experiments, we realized that participants who had fallen asleep didn't show the desired signal pattern. The signal declined gradually, whereby the zigzag remained at first (which means that movement did not cause the change) but the baseline noise level increased. Then, a phase followed where zigzags also declined, resulting in a noisy signal with sporadic zigzags. Figure 3 illustrates the difference between wake and final sleep condition. From 7 initial data sets with no zigzag pattern, two had reported to have fallen asleep. Therefore, all participants of final data acquisition were asked to stay awake during the imaging protocol which eliminated the problem. In-depth analysis of sleep pattern and the effect of aging will be reported elsewhere [20].

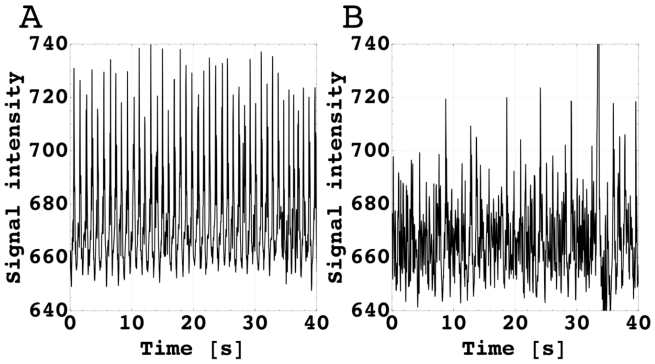

Figure 3. Pattern observed in participant who had reported falling asleep. We recognized two phases. B: First phase showed a fluctuation of the maximum peak intensity and an increase of random signals between maximum peaks. C: In the second phase, the maximum peaks decline with a further increase of the noise level between peaks. At 34 s, the peak resulted from short head movement.

We used a finger pulse oximeter and MRI data of the superior sagittal sinus to find reference time frames for the zigzag pattern. We found that the zigzags always appeared during the arterial inflow phase. The abrupt end of the zigzags were coincident with the end-phase of the arterial pulse as shown in Figure 4A and the rise of venous outflow as demonstrated in Figure 4B. The signal showed a perfect synchronization with the cardiac pulse. Therefore, the underlying mechanism of the zigzag may be a reason why a disturbence of pulse results in a vasovagal syncope [21]. Consequently, the immediate unconsciousness could be the result of the missing quantum

phenomenon.

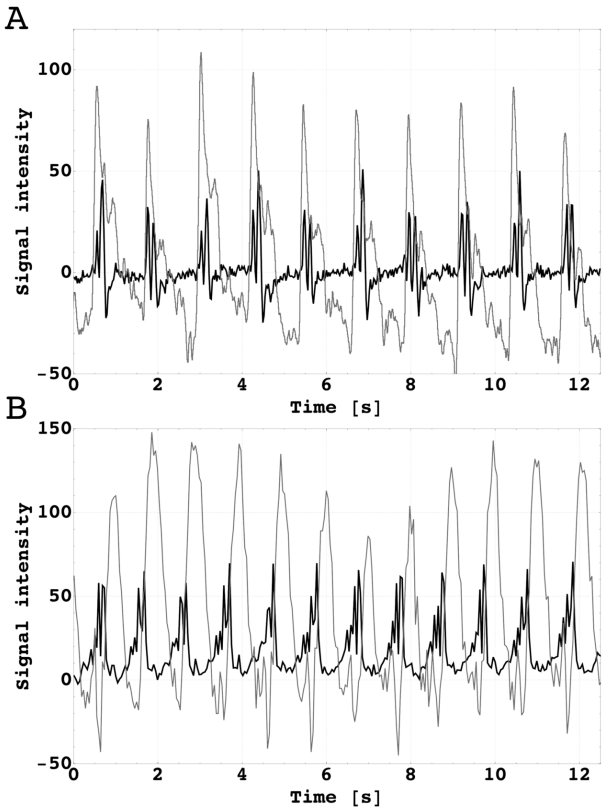

Figure 4. Signal time course (Blue) during 12 heart cycles compared with **A**: Simultaneous oximeter reading of a finger (Red) and **B**: Signal time course (Red) of a vein.

To explore the distribution over the entire brain, 9 slices (in 5 volunteers) were acquired at different positions, with slices from bottom to the top matching the position of those acquired in the anatomical scan [22]. We also wanted to prove that the signal was locally generated and not an artifact in the entire slice. For that reason, test tubes with a water solution [23] were positioned close to the head for reference signals. We located the zigzags in brain tissue of all slices except around the periventricular area (probably due to movement induced by ventricular pulsation in those regions [24].) as shown in Figure 5, regions like skull, ventricle etc and in the attached test tubes. It showed us that the signal was not generated globally which excluded external sources for the signal alteration. If possible head movements were slightly altered the zigzags disappeared in the periventricular area as well. We found this in hyperventilation challenges [25], where head movement is increased, the signal declined immediately at the start of the challenge before any cerebral blood flow response could occur. On the other hand, the effects of reduced body movements, which we realized through multiple cushions immobilizing the head and breath-holding [26] , resulted in an intermediate lengthening of the signal response (up to 4-5 peaks as in Figure 2B). Surprisingly, the signal in the breath-holding experiment did not respond to the CO_2 challenge, despite the fact, that we observed an increase of blood flow in major blood vessels during the challenge (data not shown here). Furthermore, we found in a fMRI study [27], that local increase in blood perfusion during visual activation left the zigzag undisturbed, too. We conclude from those observations that the signal was not evoked by the arterial blood flow per se.
This conforms with another interesting feature; the zigzag can be restored while being averaged over the entire tissue component of the imaging slice Figure 5A. This again requires a traveling pulse that moves faster than the blood flow. For our further analysis we made use of this highly coherent signal to calculate averaged maximum peak and baseline based on the method proposed in Gomes and Pereira [28] (over time and volume) from pre-processed data [29]. We found that the averaged maximum peak did not vary significantly with slice thickness [30] which again excludes movement as possible signal source (Figure 6A). For the imaging repetition time (TR) [31], which defines the time-of-flight, no inflow effect could be detected either (Figure 6B).

Further, we altered sequences parameters to explore the underlying contrast mechanism. First, we rotated the asymmetric gradients through slice rotation [32]. We found the characteristic angulation dependency of the dipole-dipole interaction as shown is (Figure 6C). The plot represents the fitted function $|(3 \cdot cos^2[\varphi] - 1)|$ (adjusted R^2 test of goodness-of-fit resulted in R^2=0.9958) where φ takes the additional gradients in read and phase direction into account which relates to the slice angulation as

$$\varphi = \alpha - \tan^{-1}\left[\frac{\mathrm{Gt}_{cru} - \mathrm{Gt}_{rt}}{2\mathrm{Gt}_{sat} + \mathrm{Gt}_{cru} + \mathrm{Gt}_{st}}\right] = \alpha - 9.6^\circ \ .$$

At the magic angle, the zigzag disappears completely which rules out any SQC component. Therefore, we can exclude that the zigzag was generated by changes in T_1 and T_2 relaxation, line narrowing, or magnetic field shifts. Consequently, short-range ZQC are out of question. Secondly, we varied the flip angle from 5° to 60° in steps of 5°(60°was the power limit by the specific absorption rate (SAR)). We found a maximum peak intensity at 45° (Figure 6D). The predicted signal course for iZQC [17] was fitted to the data (R^2=0.9964).
Thirdly, the distance of the REST slabs were varied between 0.8 mm and 50 mm to alter the off-resonance frequency [33]. We found a typical magnetization transfer contrast (MTC) change for the baseline signal which depended on the off-resonance frequency (Figure 6E). In contrast, the zigzag intensity showed remarkable immunity to MTC [34] with no significant changes in the same frequency range (Figure 6F).

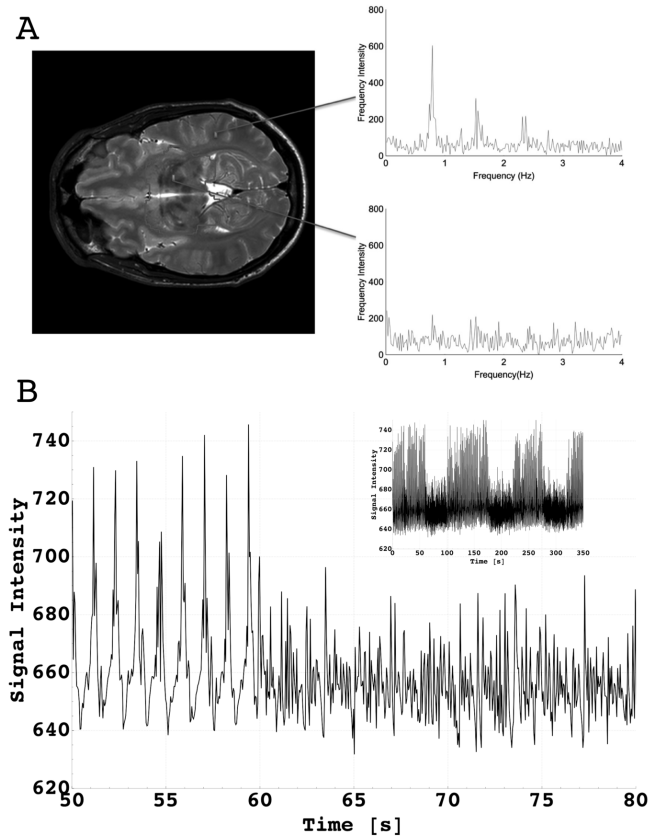

Figure 5. **A**: Fourier-Transform of two representative voxel. Surrounded tissue (gray (gr drawing) on the left shows signal dependency as shown in the bottom plot. **B**: Whole-slice averaged signal time course during normal breathing first. At 60 s, the subject was instructed to hyperventilate. The inlet shows the total time course with 3 hyperventilation periods and the selected time interval in red.

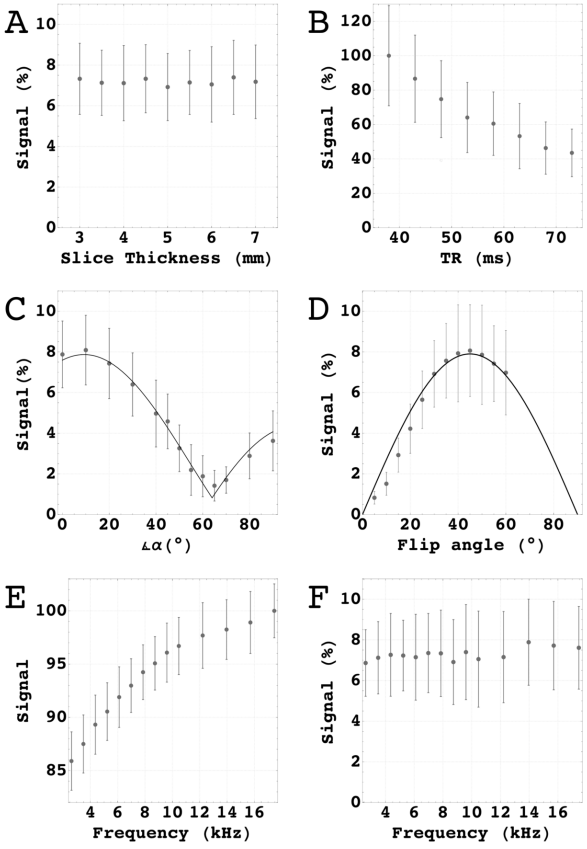

Figure 6. Variation of sequence parameters. Data shows signal averaged over 5 subjects. Error bars represent the standard deviation from the mean. **A**: Signal intensity plotted against the slice gradient angulation φ in respect to the magnetic main field. **B**: Signal intensity plotted against the frequency offset of the saturation slices of the averaged baseline signal (left) and averaged signal of cardiac pattern (right). **C**: Whole-slice averaged signal time course plotted against flip angle variation with saturation pulses (Blue) and without (Grey). IZQC prediction plotted in Red.

DISCUSSION

In summary, we have extensively shown that the zigzag is not caused by inflow nor movement nor short-range quantum coherence. Then again, the zigzag is exclusively generated by long-range ZQC. But what can alter the tissue physiology in such a way that long-range ZQC can be evoked? Broken spherical symmetries may offer such rare mechanisms which could be induced by boundaries with variable permeability. However, no alteration would extend the maximum signal of the ideal fluid which still would be nearly a magnitude smaller than our observation. We conclude that in the coherence pathway other contributions than in a classical liquid may dominate. Consequently, brain tissue cannot be treated as a classical liquid which may bring us to an exotic phase of matter. Then other observations like the instant onset and end of the zigzag period, an unaltered short-range coherence, a tendency for signal increase in time, a non-local characteristic and the dependency on the blood pressure pulse may complete the picture of a topological order. In conclusion, we believe that we have found an exotic phase of matter which could be the missing link to connecting topological defects to brain computation. Ultimately, we believe that our finding is a first experimental hint of topological quantum computing in the human brain.

Acknowledgments

We would like to thank Science Foundation Ireland for supporting D.L.P. from 2011-2015 (SFI-11/RFP.1/NES/3051).

[1] H. Atmanspacher, in *The Stanford Encyclopedia of Philosophy*, edited by E. N. Zalta (Metaphysics Research Lab, Stanford University, 2015) summer 2015 ed.

[2] S. Hameroff and R. Penrose, Mathematics and Computers in Simulation **40**, 453 (1996).

[3] M. H. Freedman, A. Kitaev, M. J. Larsen, and Z. Wang, Bulletin of the American Mathematical Society **40**, 31 (2002).

[4] N. Kumar, R. Zhang, J. J. de Pablo, and M. L. Gardel, Science Advances **4**, eaat7779 (2018).

[5] G. Duclos, C. Erlenkämper, J.-F. Joanny, and P. Silberzan, Nature Physics **13**, 58 (2016).

[6] K. Kawaguchi, R. Kageyama, and M. Sano, Nature **545**, 327 (2017).

[7] T. B. Saw, A. Doostmohammadi, V. Nier, L. Kocgozlu, S. Thampi, Y. Toyama, P. Marcq, C. T. Lim, J. M. Yeomans, and B. Ladoux, Nature **544**, 212 (2017).

[8] L. H. Kauffman and S. J. Lomonaco, New Journal of Physics **4**, 73 (2002).

[9] A. Streltsov, U. Singh, H. S. Dhar, M. N. Bera, and G. Adesso, Physical Review Letters **115** (2015), 10.1103/physrevlett.115.020403.

[10] G. Deville, M. Bernier, and J. M. Delrieux, Physical Review B (1979).

[11] G. Eska, H. G. Willers, B. Amend, and C. Wiedemann, Physica B+ C (1981).

[12] R. Bowtell, R. M. Bowley, and P. Glover, Journal of Magnetic Resonance (1969) **88**, 643 (1990).

[13] W. S. Warren, W. Richter, A. H. Andreotti, and B. T. Farmer, Science **262**, 2005 (1993).

[14] W. S. Warren, S. Ahn, M. Mescher, M. Garwood, K. Ugurbil, W. Richter, R. R. Rizi, J. Hopkins, and J. S. Leigh, Science **281**, 247 (1998).

[15] R. R. Rizi, S. Ahn, D. C. Alsop, S. Garrett-Roe, M. Mescher, W. Richter, M. D. Schnall, J. S. Leigh, and W. S. Warren, Magnetic Resonance in Medicine **43**, 627 (2000).

[16] In addition, the two saturation pulses (5 mm (15mm above and 20mm below) in thickness placed parallel to the imaged slice) (Figure 1) can increase the long-range correlation via the additional gradients of the saturation pulses by a factor of around 6.

[17] C. Zhong, Z. Shaokuan, and Z. Jianhui, Chemical Physics Letters **347**, 143 (2001).

[18] Imaging protocols were approved by the Trinity College School of Medicine Research Ethics Committee.

[19] The finalized parameters were as follows: FA = 45°, TR = 45 ms and the TE = 5 ms with a voxel size was 3.5 x 3.5 x 3.5 mm, matrix size was 64x64, SENSE factor 3, bandwidth readout direction was 2148 Hz.

[20] Lopez-Perez, "Complexity Changes of the Long-range Spin-spin Interactions in the Human Brain,".

[21] B. O. Blair P. Grubb MD, *Syncope: Mechanisms and Management*, 2nd ed. (Wiley-Blackwell, 2005).

[22] Anatomical MRI images in all studies included a high-resolution sagittal, T1-weighted MP-RAGE (TR = 2.1 s, TE = 3.93 ms, flip angle = 7).

[23] Solution composition: 1000 ml demineralized water contained 770 mg $CuSO_45H_2O$, 1 ml Arquad (AkzoNobel), 0.15 ml H_2SO_4-(0.1 N)).

[24] R. Nunes, P. Jezzard, and S. Clare, J Magn Reson **177**, 102 (2005).

[25] During indicated intervals four participants were asked to hyperventilate for 40 s.

[26] During indicated intervals the subjects were asked to stop breathing for 20 s with out taken a deep breath.

[27] D. López-Pérez, *Non-Single Quantum MRI: A Cardiac Modulated Rhythm in the Brain Tissue*, Ph.D. thesis, Medicine, Trinity College Dublin (2016).

[28] E. F. Gomes, A. M. Jorge, and P. J. Azevedo, in *Proceedings of the International C* Conference on Computer Science and Software Engineering* (ACM, 2013) pp. 23–30.

[29] Data were processed with Matlab 2014a (http://www.mathworks.co.uk/). Rescaling was applied to all data sets before any analysis using the MR vendor's instructions. Average time series were visually inspected in search for irregularities which were manually removed from the analysis leaving the rest of the time series unaltered. Manual segmentation was used to create a mask to remove cerebral spinal fluid (CSF) contributions. The first 100 of 1000 scans were removed to avoid signal saturation effects. The manual segmentation of the masks was eroded to avoid partial volume effects at the edges.

[30] Slice thickness from 3 mm to 7 mm in steps of 0.5 mm.

[31] TR varied from 38 ms to 73 ms in steps of 5 ms.

[32] Slice angulation started from coronal 0° to axial 90°in the steps as [0, 10, 20, 30, 40, 45, 50, 55, 60, 65, 70, 80, 90]; Saturation gradients had a time integral (length x strength) of Gt_{sat} = 5.1 ms x 6.25 mT/m, the crusher gradients in read and slice direction of Gt_{cru} = 1.3 ms x 25 mT/m, the slice rephase gradient of Gt_{sr} = 0.65 ms x 25 mT/m, the slice termination gradient of Gt_{st} = 0.65 ms x 15 mT/m, and the total read dephase after EPI readout gradient of Gt_{rt} = 0.65 ms x 22.5 mT/m.

[33] The off-resonance frequencies resulted in [2.62, 3.49, 4.36, 5.23, 6.11, 6.98, 7.84, 8.73, 9.60, 10.47, 12.22, 13.96, 15.71, 17.45] kHz.

[34] E. Uzi and N. Gil, Journal of Magnetic Resonance **190**, 149 (2008).